Journal of New Materials for Electrochemical Systems 14, 019-026 (2011)

Preparation, Characterization and Electrochemical Performance of $LiNi_xCo_yCu_zMn_{2-x-y-z}O_4$ as Positive Electrodes in Lithium Rechargeable Batteries

Atef Y. Shenouda[1,*], El Sayed M. El Sayed[1] and Hua K. Liu[2]

[1]Central Metallurgical Research and Development Institute (CMRDI), Tebbin, Helwan, Egypt
[2] Institute for Superconducting and Electronic Materials, ARC Centre of Excellence for Electro materials Science, University of Wollongong, NSW 2522, Australia

Received: November 01, 2010, Accepted: January 12, 2011, Available online: February 15, 2011

Abstract: *A series of spinel compounds including $LiCu_{0.25}Co_{0.25}Ni_{0.25}Mn_{1.25}O_4$ and $LiMn_2O_4$ were prepared by the sol–gel method using glycine, ethanol, and ammonia solutions. The structural and magnetic properties were examined by X-ray diffraction, Scanning Electron Microscopy, and electron spin resonance. The prepared powders have spinel-phase cubic structure with space group Fd3m. It is found that the Curie constant "C_p" and the effective magnetic moment "μ_{eff}" values decrease with the more metal doping. The electrochemical properties were characterized and found to be superior for the $LiCu_{0.25}Co_{0.25}Ni_{0.25}Mn_{1.25}O_4$. It was observed that the Warburg impedance coefficient (σ_w) was 122 $\Omega.s^{-0.5}$ for $LiCu_{0.25}Co_{0.25}Ni_{0.25}Mn_{1.25}O_4$ (sample B), which was lower than the value for $LiMn_2O_4$ (sample A), 819 $\Omega.s^{-0.5}$. Also, the diffusion coefficient (D) values of the lithium ions diffusing into the bulk electrode materials were calculated. Sample B had a higher "D" value than sample A. The prepared multi-doped lithium manganate spinel material delivered a higher specific discharge capacity of ~150 $mAhg^{-1}$ compared to 115 $mAhg^{-1}$ for $LiMn_2O_4$ after 150 cycles.*

Keywords: Lithium batteries -doped lithium positive electrode.

1. INTRODUCTION

Different types of active materials have been studied for both the positive and the negative electrodes in lithium rechargeable batteries [1-5]. Over the last few years, much work was devoted to the material/chemical aspects of $LiMn_2O_4$, $LiNiO_2$, and $LiCoO_2$ compounds [6]. Among all these systems, the $LiMn_2O_4$ system remains the most attractive in terms of cost, abundance, and non-toxicity. It has been found, however, that the capacity of $LiMn_2O_4$ is lower than those of the other systems. The theoretical capacity is about 143 mAh g^{-1} [7-9]. Due to its electronic configuration, $t_{2g}^3.e_g^1$, Mn^{3+} can induce Jahn–Teller distortion [10]. It is well known that manganese ions in $LiMn_2O_4$ are in two oxidation states, consisting of 50% Mn^{3+} and 50% Mn^{4+}.When the amount of Mn^{3+} is more than 50%, the spinel $LiMn_2O_4$ is apt to exhibit Jahn–Teller distortion [11]. During the discharge process, especially at high rates, the diffusion rate of lithium ions in the electrolyte solution is much more rapid than inside the spinel $LiMn_2O_4$ particle [12]. In non-equilibrium dynamic conditions, lithium ions heap up at the surface of spinel $LiMn_2O_4$ particles. In addition, Mn^{3+}-rich regions are formed in this process, which induces Jahn–Teller distortion. To inhibit the Jahn–Teller distortion, many research groups have tried to dope the Mn sites with other cations (Co, Ni, Cr, Fe, Cu, Mg, Al, etc.) and improved the cell capacity, as well as the cycling performance, over that of pure spinel $LiMn_2O_4$ [11-16]. This approach can partially reduce the Jahn–Teller distortion of spinel $LiMn_2O_4$ because it reduces the Jahn–Teller active Mn^{3+} content [17, 18].

There are many papers on metal cation-doped $LiMn_2O_4$, and these papers usually focus on improving the electrochemical performance and electronic conductivity of $LiMn_2O_4$ via doping with one or two cations, such as Ni, Co, Cr, Zn, etc. These efforts have achieved some success. Dahn et al. showed that lithium de-intercalation from $LiNi_{0.5}Mn_{1.5}O_4$ occurs at a potential of 4.6 - 4.7 V vs. Li^+ [19]. This reaction is attributed to the oxidation of Ni^{2+} to Ni^{4+}.

$LiNi_{0.4}Mn_{1.6}O_4$ was prepared under air and oxygen atmospheres using fine Mn_3O_4 particle and large MnO_2 particle at various temperatures [20]. The sample prepared from Mn_3O_4 at 750 °C under

*To whom correspondence should be addressed: Email: ayshenouda@yahoo.com
Fax:, 00202 25010639

air or oxygen atmosphere exhibited an ideal electrochemical behavior. electrochemical reactions of $LiNi_{0.4}Mn_{1.6}O_4$ are well explained based on three redox couples of Mn^{3+}/Mn^{4+}, Ni^{2+}/Ni^{3+}, and Ni^{3+}/Ni^{4+} by considering a presence of oxygen defects.

It was also reported that $LiCu_xMn_{2-x}O_4$ ($0.1 \le x \le 0.5$) showed a reversible electrochemical reaction at 4.95 *V*, which was attributed to the oxidation-reduction of Cu^{2+}/Cu^{3+} [21-23]. Research has been focused on the $LiCu_{0.5}Mn_{1.5}O_4$ system and its doped counterpart with Ni cations, $LiNi_xCu_{0.5-x}Mn_{1.5}O_4$ ($0 \le x \le 0.5$) spinel [23, 24]. Electrochemical results showed that the inclusion of Ni in the Cu-modified spinel increases the overall reversible capacity from 72 $mAhg^{-1}$ for $LiCu_{0.5}Mn_{1.5}O_4$ to 120 $mAhg^{-1}$ for the spinel $LiNi_{0.35}Cu_{0.15}Mn_{1.5}O_4$.

However, to the best of our knowledge there has been no attempt to investigate the electrochemical performance and behavior of $LiCu_{0.25}Co_{0.25}Ni_{0.25}Mn_{1.25}O_4$ as a multi-doped $LiMn_2O_4$ compound.

2. EXPERIMENTAL

2.1. Material preparation and sample characterization

$LiMn_2O_4$, $LiNi_{0.75}Mn_{1.25}O_4$, $LiCo_{0.75}Mn_{1.25}O_4$, $LiCu_{0.75}Mn_{1.25}O_4$, $LiCo_{0.37}Ni_{0.37}Mn_{1.25}O_4$, $LiCu_{0.37}Ni_{0.37}Mn_{1.25}O_4$, $LiCo_{0.37}Cu_{0.37}Mn_{1.25}O_4$, and $LiCo_{0.25}Cu_{0.25}Ni_{0.25}Mn_{1.25}O_4$ cathode material samples, labeled respectively as A, 1-6 and B were prepared by a sol-gel process [25]. Stoichiometric amounts for the above compounds of Li_2CO_3 (SD Fine Chem. Ltd.), Mn $(CH_3CO_2)_2$ (SD Fine Chem. Ltd.), $Cu(CH_3CO_2)_2.H_2O$ (Polarabo), $Ni(CH_3CO_2)_2.4H_2O$ (Aldrich), and $Co(CH_3\ CO_2)_2.4H_2O$ (Aldrich) were dissolved in the proper amounts, in separate dilute solutions of acetic acid or distilled water. About 50 ml ethanol was introduced into a mixture, which was heat-treated at 80 °C for 4 *h*. Ammonia solution (28 - 30%) was added to adjust the solution pH to 5.5. After that, glycine was added at twice the molar fraction of the total stoichoimetric of the starting materials, and the mixture was heated until a gel was formed [1]. The mixture was further heated to dryness, cooled, and ground into powder. The powder was transferred into a furnace and heated for 12 h in air at 800 °C.

Determination of the chemical composition of the prepared compounds was carried out by inductively coupled plasma optical emission spectroscopy (ICP-OES, PerkinElmer Optima 2000 DV). The samples were investigated by X-ray diffraction (XRD) using a Siemens diffractometer. Brunauer-Emmett-Teller (BET) surface area analysis was carried out using a Quantachrome Nova Instrument. Scanning electron microscopy (SEM) was carried out by using Joel SEM-Model 5040. Electron spin resonance (ESR) spectra were collected by using a Bruker ESR spectrometer at 293 K.

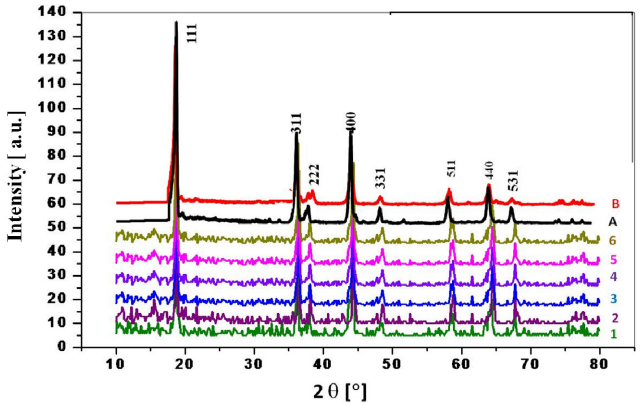

Figure 1. XRD patterns of $LiMn_2O_4$ (A), $LiNi_{0.75}Mn_{1.25}O_4$ (1), $LiCo_{0.75}Mn_{1.25}O_4$ (2), $LiCu_{0.75}Mn_{1.25}O_4$ (3), $LiNi_{0.37}Co_{0.37}Mn_{1.25}O_4$ (4), $LiNi_{0.37}Cu_{0.37}Mn_{1.25}O_4$ (5), $LiCo_{0.37}Cu_{0.37}Mn_{1.25}O_4$ (6) and $LiCo_{0.25}Cu_{0.25}Ni_{0.25}Mn_{1.25}O_4$ (B) samples.

The temperature and magnetic field dependence of the magnetization were measured in liquid nitrogen between 65 and 300 *K* with a vibrating sample magnetometer (VSM, LDJ-Electronic-Inc (Troy-MI-USA) 9600-1VSM).

2.2. Electrochemical measurements

Active material powders, carbon black, and polytetrafluoroethylene (PTFE) binder were mixed in a weight ratio of 85:5:10, respectively, to fabricate composite positive electrode material with homogeneous mixing in a mortar and pestle (agate type). The mixture was blended with a suitable amount of N-methyl-2- pyrrolidone (NMP) to yield homogeneous slurry. The slurry was then spread onto Al foil substrates. The area of a coated electrode was 1 cm^2, and the weight of the active material was about 5 mg. The electrodes were dried at 120 °C for 8 h in a vacuum oven. The electrodes were then pressed under a mechanical pressure of 1500 kg/cm^2. Coin cells were assembled in argon filled glove box. The two electrodes were the active material electrode (working electrode) and lithium metal ribbon (Sigma-Aldrich) as both counter and reference electrode. The separator was a circular foil of microporous polypropylene. The electrolyte was 1 M $LiClO_4$ dissolved in a 1:1 mixture of propylene carbonate (PC) and dimethyl carbonate (DMC), (Fluka, 99%). All potentials were recorded vs. Li/Li^+ electrode. Cyclic voltammetry (CV) measurements were performed using a Multistat CHI 660 Electrochemical Workstation at a 0.1 mVs^{-1} scanning rate, with a potential window of 2.5 to 5.5 V vs.

Table 1. Crystal unit cell parameters of the prepared A, B and the six samples.

Sample (S)	Unit cell lattice [Å]	Cell volume [$Å^3$]	FWHM β [°]	Selected *2θ* [°]	Crystallite size (*L*) [nm]	Surface area [m^2g^{-1}]	Strain (ε) $\times 10^{-3}$	Dislocation density δ [m^{-2}] $\times 10^{16}$
A	8.219	555	0.413	44.066	20.09	3.61	1.8017	1.6365
1	8.149	541	0.403	44.09	20.59	4.82	1.7578	1.5711
2	8.135	538	0.393	44.12	21.12	4.75	1.7134	1.4953
3	8.204	552	0.412	44.17	20.21	4.82	1.7911	1.6202
4	8.139	539	0.373	44.214	22.33	5.01	1.6207	1.3372
5	8.161	543	0.391	44.235	21.37	5.12	1.6935	1.4561
6	8.172	545	0.389	44.256	21.48	5.11	1.6846	1.4389
B	8.124	536	0.334	44.2697	25.05	8.25	1.4450	1.0649

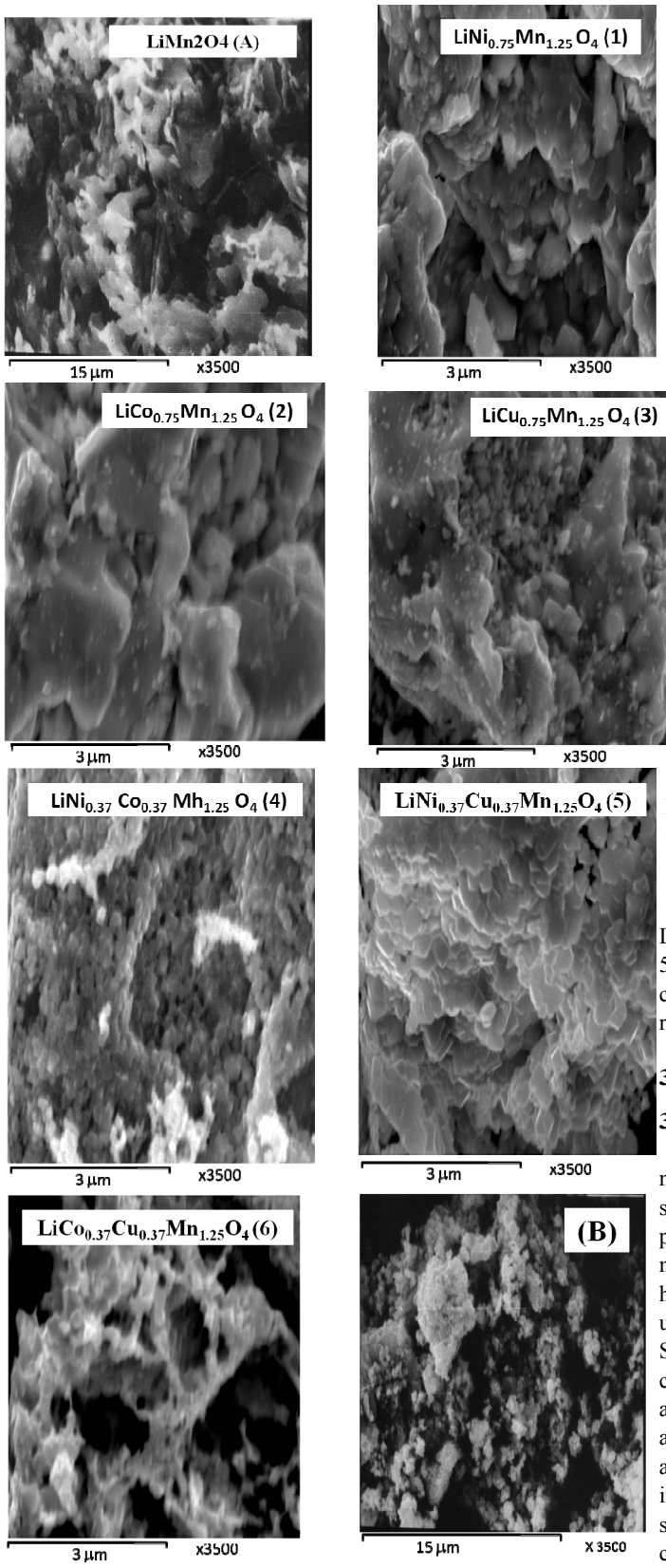

Figure 2. SEM of $LiMn_2O_4$ (A), $LiNi_{0.75}Mn_{1.25}O_4$ (1), $LiCo_{0.75}Mn_{1.25}O_4$ (2), $LiCu_{0.75}Mn_{1.25}O_4$ (3), $LiNi_{0.37}Co_{0.37}Mn_{1.25}O_4$ (4), $LiNi_{0.37}Cu_{0.37}Mn_{1.25}O_4$ (5), $LiCo_{0.37}Cu_{0.37}Mn_{1.25}O_4$ (6), and $LiCo_{0.25}Cu_{0.25}Ni_{0.25}Mn_{1.25}O_4$ (B) samples.

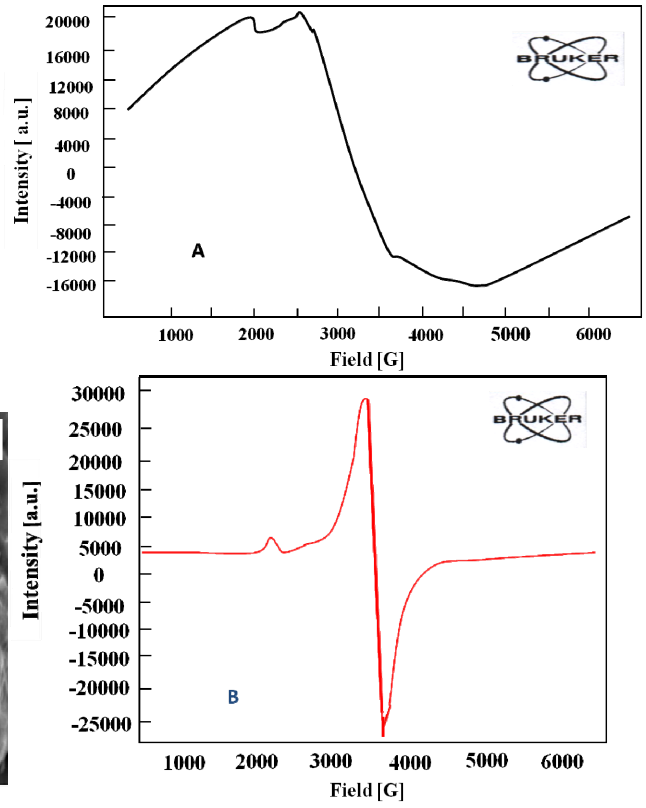

Figure 3. Electron Spin Resonance of $LiMn_2O_4$ (A) and $LiCo_{0.25}Cu_{0.25}Ni_{0.25}Mn_{1.25}O_4$ (B) samples.

Li/Li+ electrode. The AC impedance measurement amplitude was 50 mV. The frequency range was 10^5–10^{-2} Hz. The cells were charged and discharged at 0.020 A·cm^{-2} between 2.5 and 4.5 V at room temperature.

3. RESULTS AND DISCUSSION

3.1. Structural Characterization

X-ray diffraction (XRD) patterns of the six samples beside $LiMn_2O_4$ (sample A) and $LiCo_{0.25}Cu_{0.25}Ni_{0.25}Mn_{1.25}O_4$ (sample B) are shown in Fig. 1. The pattern of the $LiMn_2O_4$ sample has the distinct peaks reported in the literature [26]. Also, the other samples show mainly the same characteristic peaks. The as-prepared powders have spinel-phase cubic structure with space group Fd3m [27]. The unit cell lattice parameter, the crystallite grain size (L) using Scherer's equation, and the dislocation densities of the crystal particles are given in Table 1. It can be observed that the crystallite size and surface area increase with the doping substitution of one, two, and three transition metals, respectively. The lattice constant, a, also decreases with the introduction of more than one metallic doping substitution. This occurs especially with Co and Ni metallic substitution. However, Cu doping causes little change in the unit cell dimension and consequently the crystallite size. This is attributed to the difference in ionic radii between manganese, which is larger in the octahedral coordination, and the various dopant ions. Similar observations for these dopant metals (Co, Ni, and Cu) have been reported in the literature [28, 29]. Furthermore, the strain, ε,

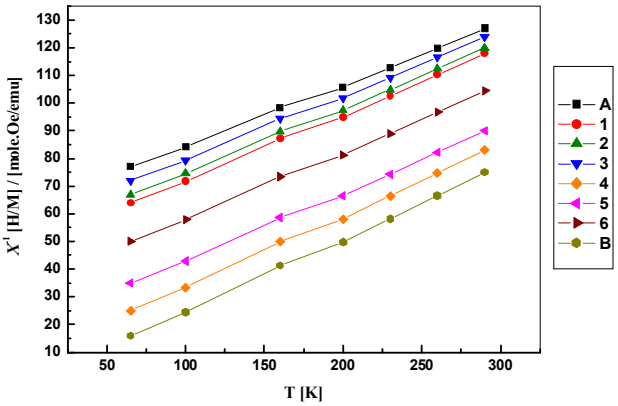

Figure 4. Dependence of the inverse magnetic susceptibility on temperature for spinel samples of $LiMn_2O_4$ (A), $LiNi_{0.75}Mn_{1.25}O_4$ (1), $LiCo_{0.75}Mn_{1.25}O_4$ (2), $LiCu_{0.75}Mn_{1.25}O_4$ (3), $LiNi_{0.37}Co_{0.37}Mn_{1.25}O_4$ (4), $LiNi_{0.37}Cu_{0.37}Mn_{1.25}O_4$ (5), $LiCo_{0.37}Cu_{0.37}Mn_{1.25}O_4$ (6), and $LiCo_{0.25}Cu_{0.25}Ni_{0.25}Mn_{1.25}O_4$, (B) compounds.

and the dislocation density, δ, of the crystals for the samples are given by the following formulas [30]:

$$\varepsilon = -\beta \cos\theta / 4 \quad (1)$$

$$\delta = 15\beta \cos\theta / 4aL \quad (2)$$

Where β is the full width half maximum (FWHM) according to the Scherer formula. It should be noted that the ε and δ values decrease with the use of more than one doping substitution.

This behavior can be explained as due to the more even arrangement and denser packing of the atoms in the crystal lattice structure, which decreases the lattice imperfections.

3.2. Morphological characterization

The morphology of the powders was observed with a scanning electron microscope (SEM) as shown in Fig. 2 for the eight samples. The SEM image of the multi-doped powder sample is quite different from that of the $LiMn_2O_4$. The morphology of the multi-doped crystals has a fine structure and small crystallite diameter. Also, the crystal particles are shaped into spherical structures. However, the morphology of the $LiMn_2O_4$ crystals has a mountain rock structure and large crystalline particles. On the other hand, in the morphology of the six numbered samples, those with single element doping, samples 1-3 are characterized by larger crystals in comparison with samples 4-6, which contain two element doping. The average particle size from the SEM morphology is about 5 μm for sample A, while samples 1-3 have particles about 2 μm in size. On the other hand, samples 4-6 containing two doping elements show an average particle size of about 300 nm. Furthermore, sample B has an average particle size of about 250 nm. Also, the active surface area of the $LiCo_{0.25}Cu_{0.25}Ni_{0.25}Mn_{1.25}O_4$ (sample B) is larger than that of the $LiMn_2O_4$ and the other six samples as observed in Table 1.

3.3. Electron paramagnetic resonance investigation

The electron paramagnetic resonance (EPR) spectra of the spinel $LiMn_2O_4$ (sample A) and the multi-doped compound (sample B) are shown in Fig. 3 (a-b). The data obtained for EPR signal of sample A consists of Lorentzian lines with parallel g-factor, $g_{\parallel} = 1.55$ and perpendicular g-factor, $g_{\perp} = 2.7$. The EPR line shows a significant broadening. The Mn^{4+}–Mn^{4+} dipolar interactions as well as the Mn^{4+}–Mn^{3+} ones contribute to the broadening of the signal. Most probably, this signal should be attributed to Mn^{4+} ions in a low symmetry crystal field. The difference in the magnetic field ΔH = 2500 G. Also, the broadening effect of Mn^{3+} on the Mn^{4+} line width is due to the antiferromagnetic interactions. These results are in good agreement with reported ones in the work of Stoyanova et. al. [32, 33]. On the other hand, the data obtained for EPR spectrum of sample B, as illustrated in Fig. 3(b) consists of narrow Lorentzian lines with $g_{\parallel} = 1.91$ and $g_{\perp} = 2.08$. The difference in the magnetic field is only 300 G. Therefore, compound B is considered more magnetic than A. It was reported that the ESR spectrum of $LiNi_{0.5}Mn_{1.5}O_4$ showed a much narrower signal (ΔH = 170 mT) centered at g = 2:0. The band has a complex shape with two components. The signal is attributed to Mn^{4+} ions, which are the only paramagnetic entities in this compound [34]. The main signal (the narrower one), ascribable to antiferromagnetically coupled Mn^{4+} ions in a Co^{3+}, Mn^{4+}-environment, possesses a Lorentzian line shape, with a g-factor of 2.004 . The decrease in ΔH gives evidence of an increase in the rigidity of the lattice with decreasing concentration of the Jahn–Teller Mn^{3+} ions and this lattice distortion experienced by the Mn^{4+} ions enhances the electrochemical properties [34].

3.4. Magnetic characterization

The temperature dependence of the magnetic susceptibility as a function of temperature for the above specimen samples is shown in Fig. 4. It was found that the low-temperature magnetic susceptibility increased with an increase in the substitution degree from one transition metal to three ones, indicating that the dominant magnetic coupling is converted from an antiferromagnetic to ferromagnetic one. i.e. the Mn^{4+}–O_2–Mn^{4+} ferromagnetic coupling increases and the antiferromagnetic Mn^{3+}–O_2–Mn^{3+} and Mn^{3+}–O_2–Mn^{4+} pairs are reduced [35]. This causes the shift of the Weiss temperature to the higher value (less negative). χ_m is given by the following equation:

$$\chi_m = C_p / (T-\theta_p) \quad (3)$$

where C_p is the Curie constant and θ_p is the Weiss temperature.

Furthermore, it is found that the Curie constant C_p decreases with the more metal doping as recorded in Table 2. Also, the experimental effective magnetic moment μ_{eff} can be found using the following formula [36-38]:

Table 2. the values of magnetic parameters for A, B and the six samples.

Sample (S)	C_p [emu.K/mole]	θ_p [K]	$\mu_{eff.}$ [μ_B]
$Li\ Mn_2O_4$ (A)	4.5	-315	6.02455
$LiCu_{0.75}Mn_{1.25}O_4$ (3)	4.326923	-281.25	5.907557
$LiCo_{0.75}Mn_{1.25}O_4$ (2)	4.245283	-254.717	5.85156
$LiNi_{0.75}Mn_{1.25}O_4$ (1)	4.166667	-233.09	5.797126
$LiCo_{0.37}Cu_{0.37}Mn_{1.25}O_4$ (6)	4.13679	-170.39	5.776304
$LiNi_{0.37}Cu_{0.37}Mn_{1.25}O_4$ (5)	4.090909	-113.151	5.744183
$LiNi_{0.37}Co_{0.37}Mn_{1.25}O_4$ (4)	3.87931	-60.9052	5.593654
$LiCo_{0.25}Cu_{0.25}Ni_{0.25}Mn_{1.25}O_4$ (B)	3.813559	-20.6695	5.546048

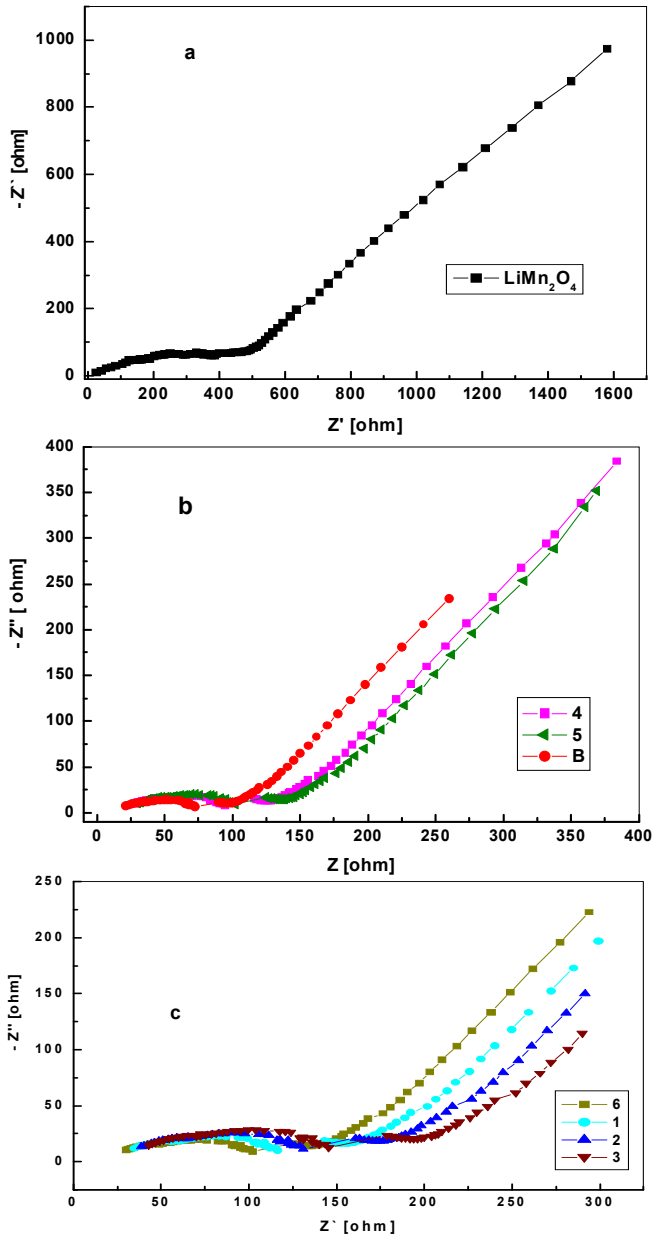

Figure 5. (a-c) EIS of $LiMn_2O_4$ (A) ; $LiNi_{0.75}Mn_{1.25}O_4$ (1); $LiCo_{0.75}Mn_{1.25}O_4$ (2); $LiCu_{0.75}Mn_{1.25}O_4$ (3); $LiNi_{0.37}Co_{0.37}Mn_{1.25}O_4$ (4) ; $LiNi_{0.37}Cu_{0.37}Mn_{1.25}O_4$ (5); $LiCo_{0.37}Cu_{0.37}Mn_{1.25}O_4$ (6) and $LiCo_{0.25}Cu_{0.25}Ni_{0.25}Mn_{1.25}O_4$ (B) cells.

$$\mu_{\text{eff}} = \mu_B \sqrt{(3k_B C_p / N_A)} \quad = 2.84\,\mu_B \sqrt{C_p} \qquad (4)$$

where: μ_B is the Bohr magneton, k_B is Boltzmann's constant, and N_A is Avogadro's number. The values of the μ_{eff}, C_p, and θ_p parameters are given in Table 2. The effective magnetic moment decreases with the more metal doping. The decreasing of C_p and μ_{eff} means that the spin decreases from S=2 for Mn^{3+} to 1.5 for Mn^{4+}.Consequentely, the oxidation of Mn ion in spinel compounds increases from A to B materials. In the Ni^{2+}, Co^{3+} and Cu^{2+}-substituted case, the magnetic dilution is not expected, some new couplings (Mn^{3+}–O^2–Ni^{2+}, Mn^{4+}–O_2–Ni^{2+}, Mn^{4+}-O_2-Co^{3+}, Mn^{4+}-O_2-Cu^{2+}, Co^{3+}-O_2-Co^{3+}, Cu^{2+}-O_2-Cu^{2+} and Ni^{2+}–O_2–Ni^{2+}) are introduced, and N^{i2+}–O_2–Ni^{2+} coupling is strong ferromagnetic one [39]. Subsequently, the compositional variation of the Curie constant becomes lower and the ferromagnetic Curie temperature attained at the compound having three doping metals takes a higher value (less negative) indicating the increasing of ferromagnetic interactions [36].

Both EPR and magnetic susceptibility measurements permit the differentiation of regions rich in lithium and manganese. The lithium–manganese distribution is of significant importance for understanding and correspondingly, for improving the electrochemical properties of $LiMn_2O_4$ and the other doped spinel compounds.

Furthermore, the increase of Mn^{4+} and decrease of Mn^{3+} ions concentration in sample "B" rather than the other samples as explained by the difference in the magnetic field "ΔH" and the magnetic parameters C_p, and θ_p, reduces the Jahn–Teller distortion of spinel $LiCo_{0.25}Cu_{0.25}Ni_{0.25}Mn_{1.25}O_4$ (sample B) in greater amount more than the other investigated samples. Similar results were obtained for $LiNi_{0.5}Mn_{1.5}O_4$, $LiNi_{0.4}Mn_{1.6}O_4$ and $LiMg_{0\cdot05}Ni_{0.45}Mn_{1.5}O_4$ [40, 41]. It was explained for these mentioned spinel materials that the disordered phase present Mn^{3+} ions in the structure, whereas in the ordered phase only Mn^{4+} and Ni^{2+} ions.

3.5. Electrochemical studies

Fig. 5 shows the electrochemical impedance spectra (EIS) of the cells. The intercept at high frequency on the real axis Z' is for the resistance of the electrolyte, R_e, and this is followed by a semicircle in the high-middle frequency region and a straight line in the low frequency region. The numerical value of the diameter of the semicircle on the Z_{real} axis is approximately equal to the charge transfer resistance, R_{ct}. The values of R_e and R_{ct} are given in Table 3. The straight line in the low frequency region is attributed to the diffusion of the lithium ions into the bulk of the electrode material, the so-called Warburg diffusion. The plot of Z_{real} versus the inverse square root of the angular frequency for the lower angular frequencies is presented in Fig. 6. The parameters of the impedance spectra

Table 3 Electrochemical impedance parameters of the cells prepared from A, B and the six samples.

S	R_e	R_{ct} [Ω]	σ [$\Omega.s^{-1}$]	D [cm^2s^{-1}]	i° [mA cm^{-2}]	C_d [F]
A	25.97	409	819.01	5.27E-14	6.27E-05	4.02E-07
B	21.23	78	122.09	2.37E-12	3.29E-04	1.16E-06
1	36.55	128	225.1	7.00E-13	2.00E-04	8.45E-07
2	38.7	136	238.07	6.25E-13	1.89E-04	7.98E-07
3	43	151	264.54	5.06E-13	1.70E-04	7.18E-07
4	26.875	971	165.14	1.30E-12	2.64E-04	1.11E-06
5	27.95	101	172.54	1.20E-12	2.54E-04	1.07E-06
6	30.1	109	185.24	1.03E-12	2.36E-04	9.95E-07

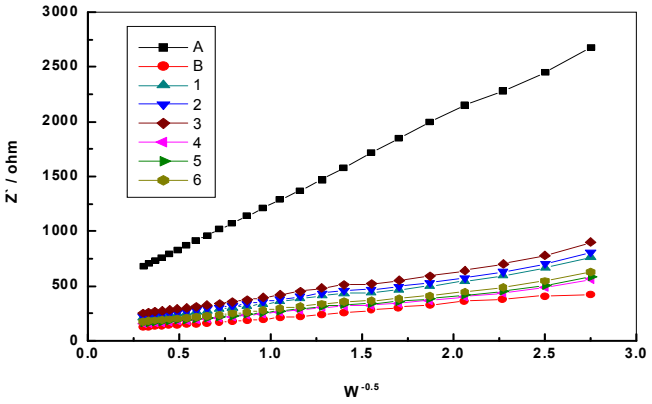

Figure 6. Relationship between real impedance (Z`) and angular frequency for $LiMn_2O_4$ (A), $LiNi_{0.75}Mn_{1.25}O_4$ (1), $LiCo_{0.75}Mn_{1.25}O_4$ (2), $LiCu_{0.75}Mn_{1.25}O_4$ (3), $LiNi_{0.37}Co_{0.37}Mn_{1.25}O_4$ (4), $LiNi_{0.37}Cu_{0.37}Mn_{1.25}O_4$ (5), $LiCo_{0.37}Cu_{0.37}Mn_{1.25}O_4$ (6), and $LiCo_{0.25}Cu_{0.25}Ni_{0.25}Mn_{1.25}O_4$ (B) cells.

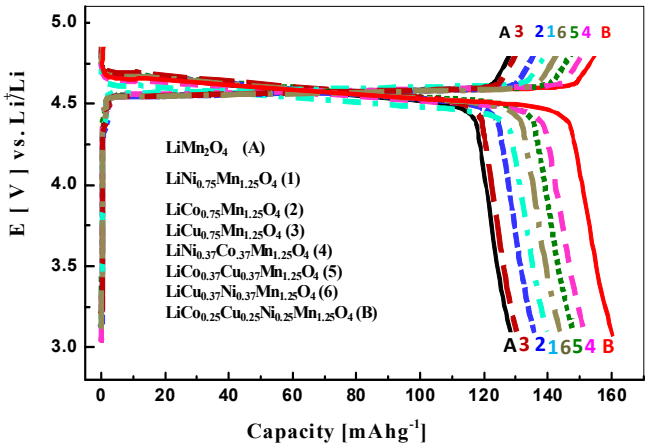

Figure 7. The potential vs. first specific discharge capacity profiles for $LiMn_2O_4$ (A), (1-6) and $LiCo_{0.25}Cu_{0.25}Ni_{0.25}Mn_{1.25}O_4$ (B) cells.

are listed in Table 3. The straight lines are attributed to the diffusion of the lithium ions into the bulk of the electrode materials, the so-called Warburg diffusion [42]. This relation is governed by equation (6) below. It is observed that the non-geometric Warburg impedance coefficient (σ_w) is 122.09 $W.s^{-0.5}$ for sample B, which is lower than the value for sample A (819.01 $\Omega.s^{-0.5}$). In addition, the diffusion coefficient values of the lithium ions diffusing into the bulk electrode materials were calculated using Equation (7) and are listed in Table 3. Sample B has a higher *D* value than sample A for Li^+ ions.

$$Z_{re} = R_e + R_{ct} + \sigma_w \cdot \omega^{-0.5} \quad (5)$$

$$D = 0.5\,(RT / A\,n^2 F^2 \sigma_w C)^2 \quad (6)$$

$$Z_{re} = R_e + R_{ct} + 2\sigma_w^2 \cdot C_{dl} \quad (7)$$

Where ω angular frequency in the low frequency region, *D*: diffusion coefficient, *R*: the gas constant, *T*: the absolute temperature, *F*: Faraday's constant, *A*: the area of the electrode surface, C_{dl}: double layer capacitance of the working electrode, and C: molar concentration of Li^+ ions. In addition, the angular frequency is given by:

$$\omega = 1 / R_{ct} \cdot C_{dl}. \quad (8)$$

Furthermore, the exchange current density ($i° = RT/nFR_{ct}$) and the double layer capacitance (C_{dl}) values of the doped sample B are higher than for sample A using equations (8) and (9). Therefore, the charge-transfer reaction in the doped spinel sample electrode takes place faster than in the electrode containing the un-doped material. On the other hand, the other samples (1-6) show impedance parameters that lie between those of samples A and B. Also, the impedance parameters with two doping elements are better than the parameters with one doping in Table 3.

The first charge - discharge capacity plateaus versus the working voltage are shown in Fig. 7. Similar results were reported [8, 41]. The first cyclic voltammogram of $LiMn_2O_4$ starts from the open circuit potential (OCP) at 3.1 V for cells A and B, respectively as shown in Fig. 8 (a-b).

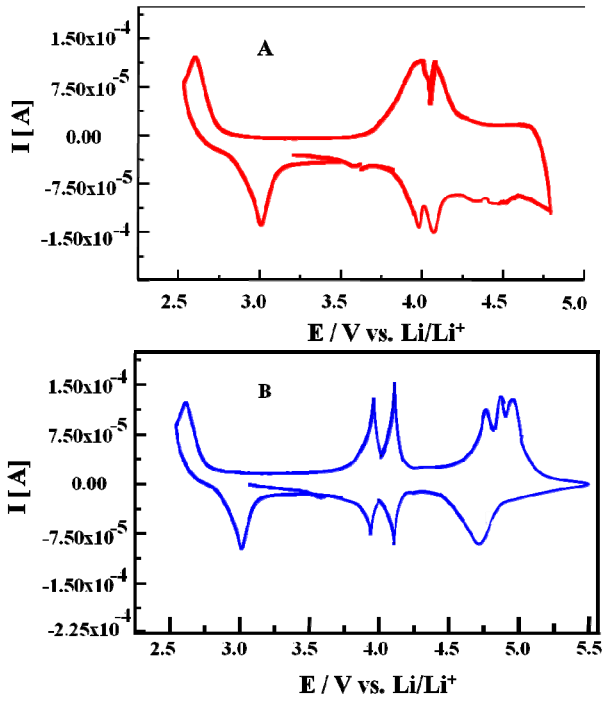

Figure 8. Cyclic voltammograms of spinel compounds $LiMn_2O_4$ (a) and $LiCo_{0.25}Cu_{0.25}Ni_{0.25}Mn_{1.25}O_4$ (b). The scan rate is 0.1 mVs^{-1}.

3.5.1. reduction process

Two peaks at 3.9 and 4.12 V for the intercalation of two Li^+ ions into the spinel phase, as explained by equations (9) and (10).

$$\lambda\text{-}MnO_2 + Li^+ \rightarrow \quad LiMn_2O_4 \quad E = 4.1\ V \quad (9)$$

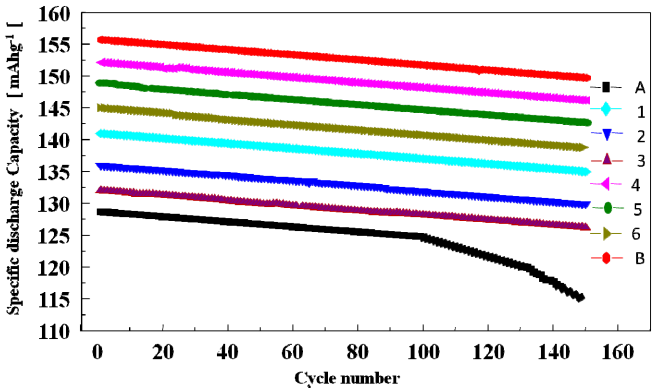

Figure 9. Cycling performance of spinel compounds of $LiMn_2O_4$ (A), $LiNi_{0.75}Mn_{1.25}O_4$ (1), $LiCo_{0.75}Mn_{1.25}O_4$ (2), $LiCu_{0.75}Mn_{1.25}O_4$ (3), $LiNi_{0.37}Co_{0.37}Mn_{1.25}O_4$ (4), $LiNi_{0.37}Cu_{0.37}Mn_{1.25}O_4$ (5), $LiCo_{0.37}Cu_{0.37}Mn_{1.25}O_4$ (6), and $LiCo_{0.25}Cu_{0.25}Ni_{0.25}Mn_{1.25}O_4$ (B) cells.

$$Li^+ + LiMn_2O_4 \rightarrow Li_2Mn_2O_4 \qquad E = 3.9\ V \qquad (10)$$

Also, another reduction peak occurs at 3 *V* due to the reduction of Mn^{3+} to Mn^{2+}, which takes place through the intercalation of one Li^+ ion into layered $LiMnO_2$:

$$Li^+ + LiMnO_2 \rightarrow Li_2MnO_4 \qquad E = 3.0\ V \qquad (11)$$

These results are in agreement with the reported ones [5, 41, 43].

3.5.2. oxidation process

Two oxidation peaks, at 4.05 and 4.17 V, occurred for the de-intercalation of Li^+ ions from $LiMn_2O_4$ to form λ-MnO_2 (equation 8) and Li^+ de-intercalation from $Li_2Mn_2O_4$ (equation 9), respectively. The de-insertion process occurs with a change in the average manganese oxidation state from 3 to 3.5. These results are in agreement with the reported ones [5, 41-44].

On the other hand, the first cyclic voltammogram (CV) curve of multi-doped lithium manganate is presented in Fig. 8 (b). It is observed that additional small anodic peaks occur at 4.62, 4.95, and 5.05 V on oxidation and 4.68, 4.77, and 5.02 V on reduction, respectively [22, 41-45]. These additional plateaus correspond to the following reactions:

$$Ni^{2+} \rightarrow Ni^{4+} + 2e \qquad E = 4.6 - 4.7\ V \text{ vs. } Li/Li^+ \text{ electrode} \qquad (12)$$

$$Cu^{2+} \rightarrow Cu^{3+} + e \qquad E = 4.9 - 4.95\ V \qquad (13)$$

$$Co^{3+} \rightarrow Co^{4+} + e \qquad E = 5 - 5.2\ V \qquad (14)$$

The multi-doped "B" sample shows a broad peak at about 4.75 V, which expresses the reduction of Ni^{4+} to Ni^{2+}, Co^{3+} to Co^{2+}, and/or Cu^{3+} to Cu^{2+} [22, 43]. It was reported that substitution of dopant for Mn ions in $LiMn_2O_4$ gives rise to a 5 V potential plateau, while the kind of substitution ion influences the 5 V behavior of $LiMe_xMn_{2-x}O_4$ (Me = Cr, Fe, Co, Ni, Cu) cathode materials [20, 44]. It was reported that the oxidation of Ni^{2+} to Ni^{3+} and Ni^{4+} gives higher potential such as 5 V behavior [41]. From the energy levels of the *d*-orbitals in Mn and Ni ions, it can be expected that a 4 V potential plateau corresponds to the redox couple of Mn^{3+}/Mn^{4+}, while the ones at 5 V are due to two redox couples of Ni^{2+}/Ni^{3+} and Ni^{3+}/Ni^{4+}. The discharge curve at 5 V involves two plateaus. The lower potential plateau is assigned to the Ni^{2+}/Ni^{3+} redox couple, and the higher one is contributed by the Ni^{3+}/Ni^{4+} redox couple. Also, the redox couples of Co^{3+}/Co^{4+} and Co^{3+}/Co^{4+} possess 5 V potentials that are in agreement with a previous reported work [41].

The cycle life performances of the numbered samples from 1 to 6, A and B are presented in Fig. 9. It shows that the multi-doped spinel material has higher discharge capacity of 150 $mAhg^{-1}$ compared to 125 $mAhg^{-1}$ for the spinel $LiMn_2O_4$ after 150 cycles. The discharge capacity of the multi-doped sample B is larger by about 15 % than that of the un-doped sample A. Also, it is observed that the six numbered samples have specific discharge capacities that lie between the multi-doped and un-doped samples. Mohamedi et. al. [46] mentioned that the electrode initially delivered a capacity of 155 mAh g^{-1}, which is very close to the theoretical capacity of 150 mAh g^{-1}, when all lithium can be extracted from $LiNi_{0.5}Mn_{1.5}O_4$. Leroux and Nazar [47] showed a specific capacity of 160 mAh g^{-1} at C/1.8 (85 mAg^{-1}) for $Li_{0.74}K_{0.02}MnO_4$. Zhang et. al. [48] showed the first charge capacity and discharge capacity are 184 and 172 $mAhg^{-1}$ for $LiNi_{1/3}Mn_{1/3}Co_{1/3}O_2$, respectively.

4. CONCLUSION

We have studied the structural, physical, and electrochemical properties of Ni, Cu and Co-substituted $Li-Co_{0.25}Ni_{0.25}Cu_{0.25}Mn_{1.25}O_4$ positive electrode materials synthesized by a sol–gel method from ammonia and glycine precursors. X-ray diffraction patterns, SEM, and magnetic measurements were carried out. XRD patterns have shown spinel-phase cubic structure with space group Fd3m. The magnetic susceptibilities, Curie constant, Weiss temperature and the effective magnetic moment increase with the more metal doping. The voltage profiles of the spinel oxide samples monitored against lithium electrode show that the overall capacity of positive electrodes was about 155 $mAhg^{-1}$ for cell B, while it was 115 $mAhg^{-1}$ for cell A. However, more stable charge–discharge cycling performances have been observed with more than 150 $mAhg^{-1}$ when electrodes are charged up to 4.5 V for cell B as compared to the performances of the native oxide cell A.

REFERENCES

[1] A.Y. Shenouda, Electrochimica Acta, 51, 5973 (2006).
[2] A.Y. Shenouda and K.R. Murali, J. Power Sources, 176, 332 (2008).
[3] A.Y. Shenouda and Hua Kun Liu, J. Power Sources, 185, 1386 (2008).
[4] A.Y. Shenouda, Hua K. Liu, Journal of Alloys and Compounds, 477, 498 (2009).
[5] A.Y. Shenouda, Hua K. Liu, J. Electrochem. Soc., 157, A1183 (2010).
[6] M. Broussely, P. Biesan and B. Simen, Electrochim. Acta, 45, 3 (1999).
[7] B. Garcia, J. Fary and J.P. Pereira-Ramos, J. Electrochem. Soc., 144, 807 (1997).
[8] J.M. Tarascon, W.R. McKinnon, F. Coowar, T.N. Bowmer, G.

Amatucci and D. Guyomard, J. Electrochem. Soc., 141, 1421 (1994).
[9] X. Fang, N. Ding, X.Y. Feng, Y. Lu, C.H. Chen, Electrochimica Acta, 54, 7471 (2009).
[10]A. Yamada, J. Solid State Chem., 122, 160 (1996).
[11]S.R. Das, S.B. Majumder, R.S. Katiyar, J. Power Sources, 139, 261 (2005).
[12]W.K. Zhang, C. Wang, H. Huang, Y.P. Gan, H.M. Wu, J.P. Tu, J. Alloys and Compounds, 465, 250 (2008).
[13]K.J. Kim, J.H. Lee, Solid State Commun., 141, 99 (2007).
[14]J. Molenda, D. Palubiak, J. Marzec, J. Power Sources, 144, 176 (2005).
[15]M. Takahashi, T. Yoshida, A. Ichikawa, K. Kitoh, H. Katsukawa, Q. Zhang, M. Yoshio, Electrochim. Acta, 51, 5508 (2006).
[16]R. Alcantara, M. Jaraba, P. Lavela, J.L. Tirado, J. Electroanal. Chem., 566, 187 (2004).
[17]P. Arora, B. Popov and R.E. White. J. Electrochem. Soc., 145, 807 (1998).
[18]P. Strobel, A.I. Palos, M. Anne, C. Poinsignon, A. Crisci, Solid State Sciences, 5, 1009 (2003).
[19]Q. Zheng, A. Bonakdarpour, M. Zhang, Y. Gao and J.R. Dahn, J. Electrochem. Soc., 144, 205 (1997).
[20]K. Kanamura, W. Hoshikawa, Solid State Ionics, 177, 113 (2006).
[21]Ein-Eli, W.F. Howard, S.H. Lu, S. Mukerjee, J. McBreen, J.T. Vaughey, M.M. Thackeray, J. Electrochem. Soc., 145, 1238 (1998).
[22]Ein-Eli, S.H. Lu, M.A. Rzeznik, S. Mukerjee, J. McBreen, M.M. Thackeray, J. Electrochem. Soc., 145, 3383 (1998).
[23]Ein-Eli, J.T. Vaughey, M.M. Thackeray, S. Mukerjee, X.Q. Yans, J. McBreen, J. Electrochem. Soc., 146, 908 (1999).
[24]Ting-Feng Yi, Jie Shu, Yan-Rong Zhu, Rong-Sun Zhu, J. Physics and Chem. Solids, 70, 153 (2009).
[25]M.M. Thackeray, W.I.F. David. P.G. Bruce and J.B. Goodenough, Mater. Res. Bull., 18, 461 (1983).
[26]F.K. Shokoohi, J.M. Tarascon, B.J. Wilkens, C.C. Chang, D. Guyomard, J. Electrochem. Soc., 139, 1845 (1992).
[27]S. Ho Park, Ki Soo Park, Yang Kook Sun and Kee Suk Nahm, J. Electrochem. Soc., 147, 2116 (2000).
[28]J. Molenda, J. Marzec, K. Swierczek, W. Ojczyk, M. Ziemnicki, M. Molenda, M. Drozdek, R. Dziembaj, Solid State Ionics, 171, 215 (2004).
[29]Y. Wei, K.B. Kim, G. Chen, Electrochim. Acta, 51, 3365 (2006).
[30]K.R. Murali, B. Jayasuthaa, Sol. Energy, 83, 891 (2009).
[31]S. Choi and A. Manthiram, J. Solid State Chem., 164, 332 (2002).
[32]R. Stoyanova, M. Gorova, E. Zhecheva, J. Phys. and Chem. Solids, 61, 609 (2000).
[33]R. Stoyanova, M. Gorova, E. Zhecheva, J. Phys. and Chem. Solids, 61, 615 (2000).
[34]E. Zhecheva , R. Stoyanova, R. Alcantara, P. Lavela, J.L. Tirado, J. Power Sources, 159, 1389 (2006).
[35]T. Nakamura , H. Demidzu, Y. Yamada, J. Phys. and Chem. Solids, 69, 2349 (2008).
[36]N. Amdouni, K. Zaghib, F. Gendron, A. Mauger, C.M. Julien, J. Magn. Mater., 309, 100 (2007).
[37]P. Jozwiak, J. Garbarczyk, F. Gendron, A. Mauger, C.M. Julien, J. Non-Cryst. Solids, 354, 1915 (2008).
[38]K. Zaghib, A. Mauger, F. Gendron, C.M. Julien, Solid State Ionics, 179, 16 (2008).
[39]H. Demidzu, T. Nakamura, Y. Yamada, J. Magnetism and Magnetic Materials, 322, 1816 (2010).
[40]S. Patoux, L. Sannier, H. Lignier, Y. Reynier, C. Bourbon, S. Jouanneau, F. Le Cras, S. Martinet, Electrochim. Acta, 53, 4137 (2008).
[41]U. Lafont , C. Locati, W.J.H. Borghols, A. Łasin´ skac, J. Dygas, A.V. Chadwick, E.M. Kelder, J. Power Sources, 189, 179 (2009).
[42]A.J. Bard, L.R. Faulkner, Electrochemical Methods, 2nd ed., John Wiley & Sons, New York, 2001, p.231.
[43]R. Rougier, K.A. Striebel, S.J. Wen and E.J. Cairns, J. Electrochem. Soc., 145, 2975 (1998).
[44]A. Striebel, R. Rougier, C.R. Horne, R.P. Reade and E.J. Cairns, J. Electrochem. Soc., 146, 4339 (1999).
[45]H. Kawai, M. Nagata, H. Kageyama, H. Tukamoto, A.R. West, Electrochim. Acta, 45, 315 (1999).
[46]M. Mohamedi, M. Makino, K. Dokko, T. Itoh, I. Uchida, Electrochimica Acta, 48, 79 (2002).
[47]F. Leroux, Linda F. Nazar, Solid State Ionics, 100, 103 (1997).
[48]X. Zhanga, A. Maugera, Qi Lu, H. Groult, L. Perrigaud, F. Gendron, C.M. Julien, Electrochimica Acta, 55, 6440 (2010).